

## Effect of Corrosion Product Films Induced by Tensile Stress on P110 Casing Steels Induced in CO<sub>2</sub> Environment

Yangzhong Jing, Shuliang Wang, Yuyao Chen, Mingyu Bao, Li Liu \*

School of Materials Science and Engineering, Southwest Petroleum University, 8 Xindu Avenue, Chengdu, Sichuan 610500, China

\*E-mail: [liuliswpu@163.com](mailto:liuliswpu@163.com)

Received: 17 April 2018 / Accepted: 29 May 2018 / Published: 5 July 2018

---

Corrosion product films were formed on P110 casing steels by high-temperature and high-pressure autoclave in a CO<sub>2</sub> environment induced by tensile stress. The effects of applied tensile stress on the protection characteristics and electrochemical performance of the corrosion product films were investigated. Scanning electron microscopy, X-ray diffraction, and electrochemical workstation were employed to analyse the surface morphology, phase composition, electrochemical impedance spectroscopy, potential dynamic polarisation curve and Mott–Schottky curve of the corrosion product films formed on P110 casing steels in 3.5 wt.% NaCl solution of saturated CO<sub>2</sub> environment. Results showed that the integrated corrosion product films formed on P110 casing steels as induced by tensile stress, and the phase of these films was not changed. The applied tensile stress can result in smaller grain size of corrosion product films, increased grain boundaries and appearance of micro channels. Consequently, the corrosion potential showed a negative shift and the corrosion current density was considerably increased. Meanwhile, the charge transfer resistance decreased, and the concentration of carrier increased owing to the P110 corrosion product films in 3.5 wt.% NaCl solution filled with saturated CO<sub>2</sub>.

---

**Keywords:** P110 casing steels, CO<sub>2</sub> environment, Tensile stress-induced, Corrosion product films, Electrochemistry

### 1. INTRODUCTION

The corrosion of carbon steels in CO<sub>2</sub> environments has been a significant problem that cannot be ignored in the oil and gas industry. The carbon dioxide gas easily dissolves in water or water vapour, which can cause the generation of acid corrosive medium, leading to serious corrosion destruction of oil well pipes. This corrosion of carbon steel has threatened the safe production of oil and gas [1,2]. The CO<sub>2</sub>-enhanced oil recovery process is widely operated in the petroleum industry, but this leads to

the presence of a large amount of wet CO<sub>2</sub> in crude oil. In this environment, a layer of FeCO<sub>3</sub> corrosion product films will form on the surface of casing steels. The stability and integrity of the corrosion product films play a decisive role in the further corrosion of the casing steels [3–5]. The formation and performance of corrosion product films on casing steels are influenced by many factors, including temperature, CO<sub>2</sub> partial pressure, pH value, and flow rate [6]. Meanwhile, in oil wells, the casing steels are always subjected to various stresses, including tensile stress, compressive stress, shear stress, bending stress and twisting stress, due to complicated geologic structures. These loads usually cause large deformation displacement of the casing steels, resulting in elasticity or plastic deformation and high residual stress [7,8].

Research [9,10] shows that the corrosion product films have positive mechanical properties and protective effect only when they have dense crystal structure, which can fully cover the surface of metal substrates. The loading tensile stress will damage the crystal structure of the corrosion product films. As the tensile stress increases, the porous structure in the corrosion product films will expand, which results in the increase of micro-cracks. When the casing steels are subjected to plastic strain, it can reduce the power requirement of casing steels to undergo anodic dissolution. With the increase of tensile strain, casing steel corrosion can easily occur, and the protection of product films become worse [11–13]. Recent research has not yet understood the electrochemical performance of corrosion product films on P110 casing steels induced by tensile stress in CO<sub>2</sub> environment. Thus, evaluating the comprehensive performance of corrosion product films induced by tensile stress is necessary.

This work aims to determine the electrochemical behaviour of corrosion product films of P110 oil tube steels in high-temperature and high-pressure brine solution dissolved with CO<sub>2</sub> under tensile stress, including elastic stress and plastic stress, which are loaded by four-point loaded specimen holders. SEM is used to observe surface morphology, whereas XRD is used to analyse the phase composition of the corrosion product films. The electrochemical properties of P110 steels with corrosion product films in 3.5% NaCl solution dissolved with saturated CO<sub>2</sub> were studied by electrochemical test including, potentiodynamic polarisation curves, EIS and Mott–Schottky (M–S) curves. The results illustrate the influence of tensile stress on the electrochemical properties of corrosion product films of P110 steels in CO<sub>2</sub> environment. These results help understand the effect of the structures and properties of corrosion product films induced by tensile stress. Furthermore, this study is expected to provide a reasonable reference for the safety design and corrosion margin of P110 casing steels in complex stress corrosion environment.

## 2. EXPERIMENTAL

### 2.1 Material and environment

All experimental samples in this work were cut from P110 oil tube steels via wire-electrode cutting. The chemical compositions listed in Table 1 were detected by spectroscopic methodology. The metallographic structure of P110 steels are tempered sorbite, which small spherical carbide particles are dispersed uniformly in the phase of ferrite substrate, as shown in Fig. 1. The test results of

metallographic structure are shown in Table 2. The tempered sorbite type of structure has excellent comprehensive properties. The tensile curve in Fig. 2 was obtained from an electronic tensile testing machine. The results in Table 3 reveal that the yield strength ( $\sigma_s$ ), tensile strength ( $\sigma_b$ ) and elastic modulus of P110 steels are 804 MPa, 866 MPa and 206 GPa, respectively, which were calculated by the stress–strain relationship.

**Table 1.** Composition of P110 steels (mass fraction, %)

Element	C	Si	Mn	Ni	Cr	Mo	Ti	Fe
Content (wt. %)	0.26	0.25	1.71	0.02	0.05	0.01	0.01	Balance

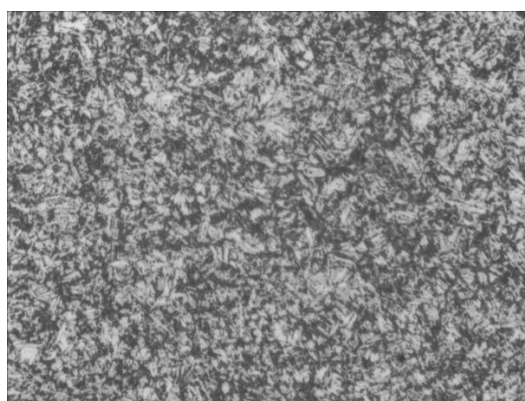


**Figure 1.** Metallographic structure of P110 steels (500×)

**Table 2.** Test results of metallographic structure

Material	Metallographic structure	Grain size number	Average grain diameter $d/mm$
P110 steels	tempered sorbite	5.5	0.02361

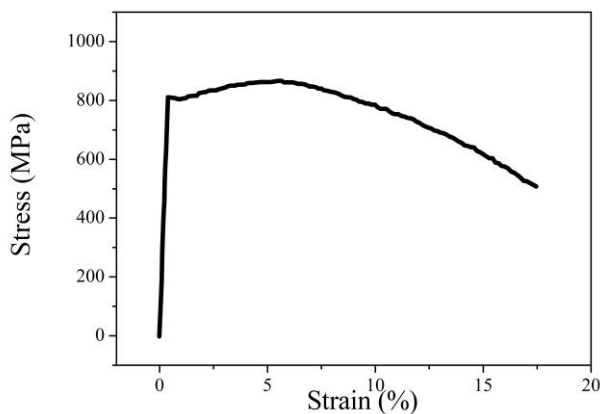


**Figure 2.** Stress–strain curve of P110 steels

**Table 3.** Test result of tensile mechanical properties of P110 steels

Material	Yield strength ( $\sigma_s$ ) MPa	Tensile strength ( $\sigma_b$ ) MPa	Elastic modulus ( $E$ ) GPa
P110 steel	804	866	206

The specimens were processed to dimension of 74 mm × 10 mm × 2 mm by wire-cut electrical discharge machine. They were polished subsequently up to 1000 grit silicon carbide paper. The surface was then rinsed with acetone and anhydrous ethanol successively, and N<sub>2</sub> was used to blow the surface dry.

Four-point loaded specimen holders were used to produce constant deformation of specimens [14]. To avoid the galvanic corrosion between the specimens and the holders, the specimens are electrically isolated from holders by a glass rod or PTFE bar. Fig. 3 shows the commonly used four-point loaded specimen holder schematic.

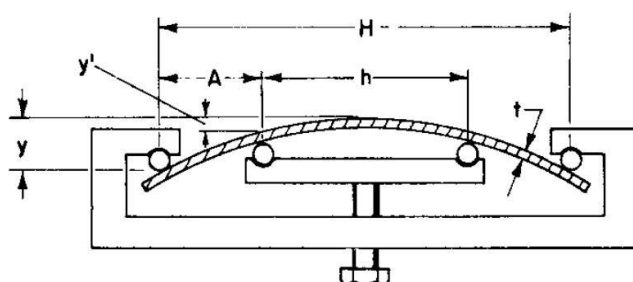


**Figure 3.** Schematic of four-point bending jigs

The elastic stress for the midportion of the specimen (between contact points of the inner support) in the outer fibres of four-point loaded specimens is calculated from the following relationship:

$$\sigma = \frac{12Ety}{3H^2 - 4A^2} \tag{1}$$

where,

$\sigma$  = maximum tensile stress,

$E$  = modulus of elasticity,

$T$  = thickness of specimen,

$y$  = maximum deflection (between outer supports),

$H$  = distance between outer supports,

$A$  = distance between inner and outer supports.

The dimensions are often chosen so that  $A = H/4$ .

The corrosion sensitivity of the corrosion product films formed by P110 steels induced by tensile stress can be compared by loading different stress levels using the four-point loaded specimen holders. The loading tensile stress values selected in this paper are shown in Table 4.

**Table 4.** Loading tensile stress of P110 steels

Stress state	0% $\sigma_s$	90% $\sigma_s$	103% $\sigma_s$
$\sigma$ (MPa)	0	723	828

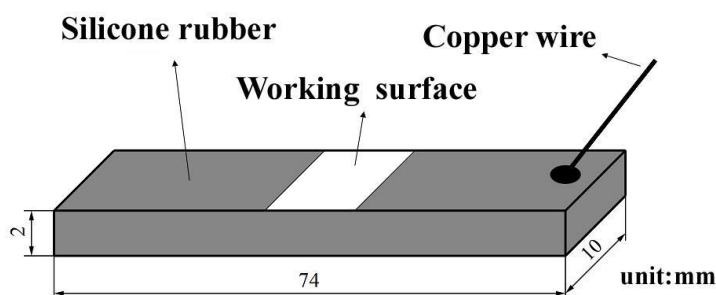
The formation of the corrosion product films are carried out in the WHF-25 Hastelloy alloy high-temperature and high-pressure static autoclave. The corrosive medium was 3.5 wt.% of the NaCl solution volume (2.5 L). The solution has been deoxidised for 4 h in advance and then sealed in the autoclave to continuously deoxidise with N<sub>2</sub> for 1 h. The experiment temperature was controlled at 90 °C, and the total pressure was maintained constantly at 5 MPa. The partial pressure of CO<sub>2</sub> and N<sub>2</sub> were 1 and 4 MPa, respectively, and the corrosion time of this experiment was 72 h. After the experiment, the specimens were removed from the holders, and the surface was rinsed and cleaned by de-ionised water and anhydrous ethanol, successively.

## 2.2 SEM and XRD

The microtopography of the corrosion product films was observed by a JSM-6490LV scanning electron microscope (SEM), and the phases of the corrosion product films were analysed by DX-2000 X-ray diffractometer (XRD).

## 2.3 Electrodes and solutions

The three-electrode system was adopted in this paper. The electrolytic pool is a glass electrolytic cell. The working electrode is shown in Fig. 4. A saturated calomel electrode (SCE) was used as reference electrode, and a platinum plate was used as the counter electrode. All experiments in this paper were conducted in 3.5 wt.% NaCl solution saturated with CO<sub>2</sub>.

**Figure 4.** Schematic of working electrode

## 2.4 Potentiodynamic polarization and EIS measurements

All electrochemical measurements were carried out by a PARSTAT 2273 electrochemical workstation. The temperature was kept at 25±1 °C in water bath. The potentiodynamic polarization

tests were measured from -300 mV below OCP to +300 mV above OCP, and the scanning rate is  $1 \text{ mV} \cdot \text{s}^{-1}$ . The EIS measurements were conducted over the frequency from 100 kHz to 10 mHz using a sine wave signal with a potential amplitude of 10 mV at OCP.

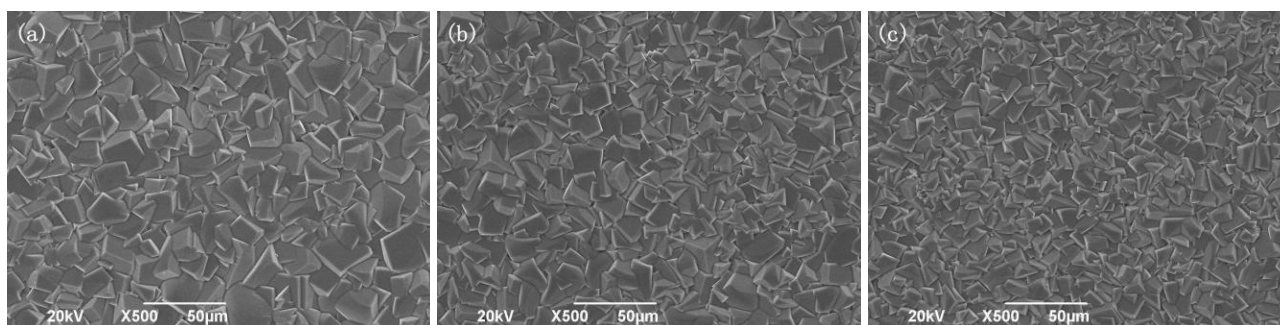
### 2.5 Mott-Schottky measurements

Mott-Schottky analysis was employed to characterize the semiconducting properties of the corrosion product films formed on the steels. The Mott-Schottky plots were obtained by sweeping from -500 mV below OCP to +500 mV above OCP at the frequency of 1 kHz with an amplitude signal of 5mV, and the scanning rate is  $50 \text{ mV} \cdot \text{s}^{-1}$ .

## 3. RESULTS AND DISCUSSION

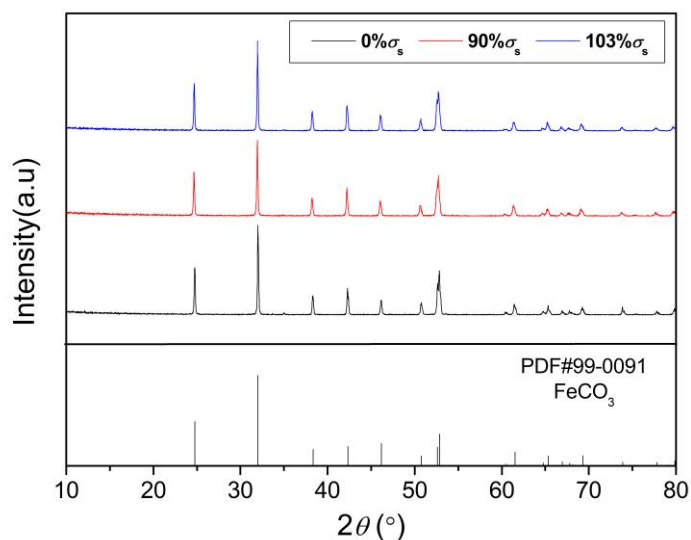
### 3.1 Analysis of corrosion product films induced by tensile stress

Fig. 5 shows the surface micromorphology of the P110 corrosion product films induced by different tensile stress formed in high-temperature and high-pressure  $\text{CO}_2$  environment. The surfaces of all specimens were covered by corrosion product films, which are composed of stacked rhombohedron crystals. Without applied tensile stress (Fig. 5(a)), the grain size of corrosion product films is large, and the grains can fully cover the P110 substrate evenly and densely. When the large elastic strain was loaded on P110 steels, the tensile stress reached  $90\% \sigma_s$ . Fig. 5(b) shows that the size of some grains becomes smaller, and the coverage of grains presents uneven on the substrate. When the tensile stress increased to  $103\% \sigma_s$ , plastic deformation occurred. Fig. 5(c) shows that the grain size of corrosion product films becomes very small, and these small grains were distributed irregularly on the surface of P110 steels. Due to the loading of plastic strain, the specimen has reached yield stage, and crystal deformation occurred in the material, causing the irreversible deformation of the lattice. The presence of tiny crystals on corrosion product films is due to tensile stress. Many nucleation positions appear during the corrosion process. Loading tensile stress has influenced the growth of corrosion product films, hindering the rest of the nucleation position where the corrosion product film has grown. Therefore, the grain size of the corrosion product films decreased, which was described in previous papers [15,16].



**Figure 5.** SEM micro-graphs (500 $\times$ ) showing the morphology of corrosion product films on P110 steels in  $\text{CO}_2$  environment induced by tensile stress (a)  $0\% \sigma_s$ ; (b)  $90\% \sigma_s$ ; (c)  $103\% \sigma_s$

Fig. 6 exhibits the XRD spectra of the corrosion product films formed on P110 steels in CO<sub>2</sub> environment induced by tensile stress. Results show that the main composition of the corrosion product films induced by different tensile stress are all FeCO<sub>3</sub>, indicating that tensile stress does not change the phase composition of the corrosion product films formed on P110 steels in CO<sub>2</sub> environment.



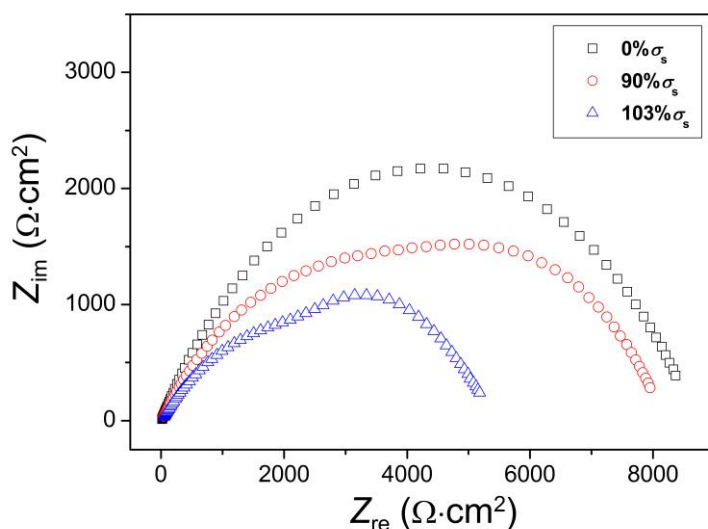
**Figure 6.** XRD spectra of corrosion product films on P110 steels in CO<sub>2</sub> environment induced by tensile stress

### 3.2 Analysis of EIS

Fig. 7 shows the Nyquist plots of P110 steels with corrosion product films formed under different tensile stresses in 3.5 wt.% NaCl solution containing saturated CO<sub>2</sub>. Fig. 7 shows that without applying tensile stress, only one capacitive reactance arc exists on the Nyquist plot, which indicates that the EIS curve has only one time constant. On this condition, the structure of the corrosion product films was dense and thick, and the main reaction of the system is between the interface of the corrosion product films and the corrosive mediums. When the value of tensile stress increases to 90%  $\sigma_s$  and 103%  $\sigma_s$  respectively, Nyquist diagrams comprise of a high-frequency capacitive loop and a low-frequency capacitive loop. With increasing tensile stress, the radii of both loops decrease, and the time constant of EIS curve induced by tensile stress is changed from one to two. Feng and coworkers [17] reported that tensile stress created the micro-cracks on the surface, also the corrosion product films would be damaged. Bai and coworkers [9] holds the same idea that pitting of the steel could lead to additional capacitive reactance in impedance spectrum and the electrode reaction process are controlled by ions diffusion in corrosion product films. So the appearance of the second time constant is mainly because of the mass of grain boundaries and micro-channels in the corrosion product film caused by the induced tensile stress. Thus, the corrosive media can reach the interface between corrosion product films and substrate through these microscopic channels. The second time constant is probably related to the corrosive reaction that happened on the interface, and the corresponding

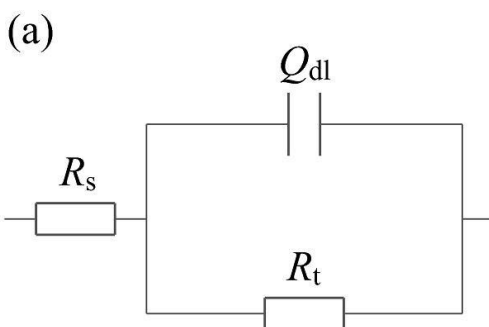
electrode reaction resistance appeared as Zhu and Sun proposed [1,10].

Table 5 shows the EIS parameters fitted by ZSimpWin software, and the equivalent circuit model for the corrosion system is shown in Fig. 8, where  $R_s$  represents solution resistance,  $R_f$  is the resistance of corrosion product films,  $Q_f$  represents the constant phase angle element of the films capacitance,  $Q_{dl}$  is the double layer capacitance and  $R_t$  represents the charge transfer resistance. Figs. 8(a) and 8(b) respectively correspond to the electrode reaction process of specimens which are without tensile stress (0%  $\sigma_s$ ) and with applied tensile stress (90%  $\sigma_s$  and 103%  $\sigma_s$ ) in 3.5 wt.% NaCl solution containing saturated  $CO_2$ .



**Figure 7.** Nyquist plots of corrosion product films on P110 steels in  $CO_2$  environment induced by tensile stress

The parameters in Table 5 indicate that with the increase of tensile stress, the charge transfer resistance ( $R_t$ ) decreases gradually. This result is because the induced tensile stress can increase the number of grain boundaries and transfer channels for ions [17], which can easily get through the corrosion product films. The tensile stress will reduce the protective effect of films; thus, the response of the impedance decreases, and corrosion is easier to occur.



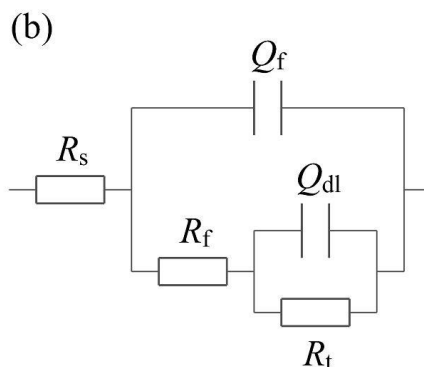


**Figure 8.** The equivalent circuit diagram of the electrochemical impedance spectroscopy of corrosion products film on P110 steels in CO<sub>2</sub> environment induced by tensile stress (a) 0%  $\sigma_s$ ; (b) 90%  $\sigma_s$  and 103%  $\sigma_s$

**Table 5.** EIS parameters of corrosion products film on P110 steels in CO<sub>2</sub> environment induced by tensile stress

Tensile stress	$R_s$ $\Omega \cdot \text{cm}^2$	$Q_f$ $\Omega^{-1} \cdot \text{cm}^{-2} \cdot \text{s}^{-n}$	$n$	$R_f$ $\Omega \cdot \text{cm}^2$	$Q_{dl}$ $\Omega^{-1} \cdot \text{cm}^{-2} \cdot \text{s}^{-n}$	$n$	$R_t$ $\Omega \cdot \text{cm}^2$
0% $\sigma_s$	9.75	---	---	---	$3.108 \times 10^{-5}$	0.5916	8684
90% $\sigma_s$	9.69	$1.762 \times 10^{-5}$	0.5346	5705	$1.311 \times 10^{-4}$	0.6887	2479
103% $\sigma_s$	10.92	$4.496 \times 10^{-5}$	0.4687	4043	$1.261 \times 10^{-4}$	0.9194	1397

### 3.3 Analysis of polarisation behaviour

Fig. 9 shows the potentiodynamic polarisation curve of P110 steels covered with corrosion product films. The parameters fitted with polarisation curves are shown in Table 6. The specimens in 3.5 wt.% NaCl solution containing saturated CO<sub>2</sub> are mainly controlled by the cathode process with or without tensile stress.

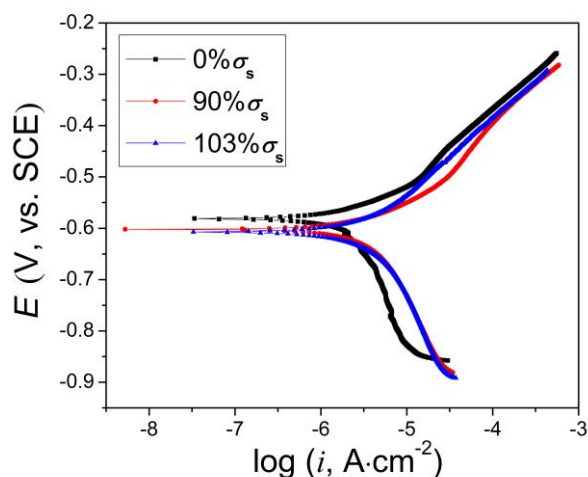


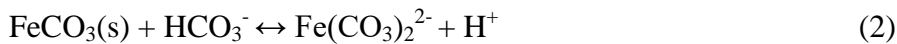
**Figure 9.** Polarisation curves of corrosion products film on P110 steels in CO<sub>2</sub> environment induced by tensile stress

**Table 6.** Polarisation curves parameters of corrosion products film on P110 steels in CO<sub>2</sub> environment induced by tensile stress

Tensile stress	$b_a$ mV·decade <sup>-1</sup>	$b_c$ mV·decade <sup>-1</sup>	$R_p$ $\Omega \cdot \text{cm}^2$	$i_{\text{corr}}$ $\mu\text{A} \cdot \text{cm}^2$
0% $\sigma_s$	146	-233	10163	3.84
90% $\sigma_s$	114	-241	7793	4.32
103% $\sigma_s$	147	-228	8882	4.38

Hausler and Stegmann [18] discussed that the existence of corrosion product films has influence on the corrosion mechanism of steels. They considered that the CO<sub>2</sub> corrosion mechanism of P110 steels can be divided into interface mechanism and interphase mechanism. The interphase mechanism holds that if dense protective films can form on the surface of the metal substrate, corrosion is a necessary condition to occur. That is, the corrosive medium must arrive at the metal substrate through the films, and then the corrosion process can be accomplished.

Under the condition of this experiment, the FeCO<sub>3</sub> corrosion product films will be dissolved and destroyed in the carbonic acid [19]. These conditions are expressed by reactions (2) and (3):



At the same time, the corrosion product films have certain ion selectivity. Chen and coworkers [20] reported that the corrosion product films formed by FeCO<sub>3</sub> crystal have an anion selective permeability. Equations (4), (5) and (6) show that the HCO<sub>3</sub><sup>-</sup>, Cl<sup>-</sup> and other anions can easily reach the interface of corrosion product films, and substrates cross micro-channels preferentially.



Without induced tensile stress, the morphology of corrosion product films is relatively compact, which has favourable protection to the metal substrate. The main reaction at this time is the dissolution of corrosion product films in carbonic acid. The leading role of cathodic reaction is the reduction of H<sub>2</sub>CO<sub>3</sub> and HCO<sub>3</sub><sup>-</sup>, which states that the cathode polarisation process is the controlling step. The SEM pictures in 3.1 indicate that induced tensile stress will decrease the grain sizes of corrosion product films, and many grain boundaries and micro-channels appear. This results in the increase of the effective reaction area of the cathodic processes and reduction of charge transfer resistance. The aggressive anions in the solution can easily pass through the micro-channels and be adsorbed on the interface of corrosion product films and the substrate [20], causing further corrosion damage of P110 steels.

Fig. 9 shows no obvious passivation in the reactions, which means the reactions are controlled by ionic activity. According to Gutmann's [21] theory of metal–mechanical chemistry and corrosion, the increase of the defects in the corrosion product films will increase the electrochemical activity of the electrode. Also Sarkar and Aquino [22] discussed the tensile stress significantly affected the evolution of the anodic dissolution front, they believed that the elastic stress would accelerate the electrochemical reaction rates. The induced tensile stress can accelerate the formation of micro-cell corrosion

[8], leading to the negative shift of the corrosion potential and the increase of the self-corrosion current density ( $i_{\text{corr}}$ ). This finding indicates that with the increase of tensile stress, the protection of corrosion product films on the substrate becomes worse, and the corrosion degrees of P110 steels in 3.5 wt.% NaCl solution containing saturated  $\text{CO}_2$  become more serious.

### 3.4. Analysis of Mott–Schottky

$\text{FeCO}_3$  corrosion product films have semi-conducting properties, and the type and concentration of carriers can be represented by M–S curves [23]. The charge distribution at the semiconductor and solution is usually determined based on M–S relationship by measuring electrode capacitance  $C_{\text{sc}}$ , as a function of electrode potential  $E$  [24]:

For n-type semiconductor:

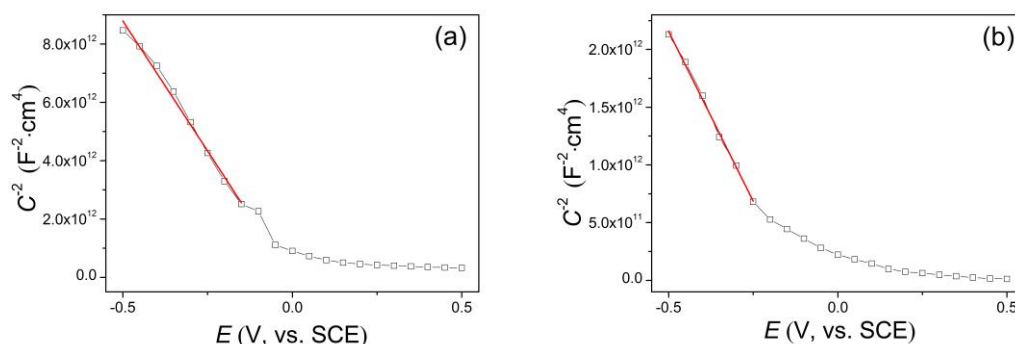
$$\frac{1}{C^2} = \frac{2}{\epsilon_0 \epsilon_r e N_D A^2} \left( E - E_{\text{fb}} - \frac{kT}{e} \right) \tag{7}$$

For p-type semiconductor:

$$\frac{1}{C^2} = \frac{2}{\epsilon_0 \epsilon_r e N_A A^2} \left( E - E_{\text{fb}} - \frac{kT}{e} \right) \tag{8}$$

where  $e$  is the electron charge ( $-1.602 \times 10^{-19}$  C),  $\epsilon_0$  is the vacuum permittivity ( $8.854 \times 10^{-14}$   $\text{F}\cdot\text{cm}^{-1}$ ),  $\epsilon_r$  is the dielectric constant of the passive film (the value in this paper is  $70 \text{ F}\cdot\text{cm}^{-1}$ ) [25],  $E_{\text{fb}}$  is the flat band potential ( $V_{\text{SCE}}$ ),  $k$  is the Boltzmann constant ( $1.38 \times 10^{-23}$  J/K),  $T$  is the absolute temperature,  $N_D$  is the donor density for n-type semiconductor ( $\text{cm}^{-3}$ ),  $N_A$  is the acceptor density ( $\text{cm}^{-3}$ ),  $A$  is the surface area of the sample ( $\text{cm}^2$ ). By the M–S equations,  $C_{\text{sc}}^{-2}$  and  $E$  is a linear relationship, which is shown as a straight line in M–S curves. The linear slope of n-type semiconductor is positive, and the slope of p-type semiconductor is negative.  $N_D$  and  $N_A$  can be determined from the slope of the experimental  $C_{\text{sc}}^{-2}$  versus  $E$  plots.

Fig. 10 shows the M–S curves of the corrosion product films on P110 steels in  $\text{CO}_2$  environment induced by tensile stress. Fig. 10 shows that the slope of the M–S curves are negative when induced by different tensile stresses, indicating that the semiconductor type of the  $\text{FeCO}_3$  corrosion product films are p-type. In the p-type semiconductor, the holes are the major carriers and the free electrons are the minor carriers.



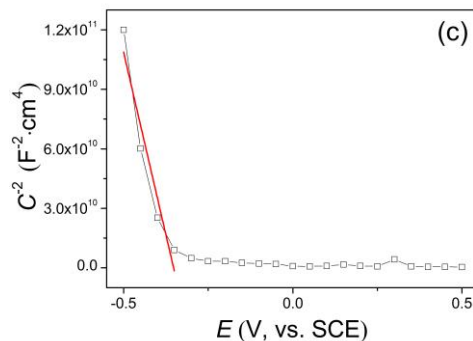


**Figure 10.** Mott–Schottky curves of corrosion product films on P110 steels in CO<sub>2</sub> environment induced by tensile stress (a) 0%  $\sigma_s$ ; (b) 90%  $\sigma_s$ ; (c) 103%  $\sigma_s$

It is investigated that the different types of passive films exhibit various semiconductor properties depending on the predominant defect present in the passive film, only p-type or n-type semiconductor is not directly related to corrosion resistance [26]. Corrosion potential and current are still the important parameters to determine the degree of corrosion, and they are directly related to the flat band potential and carrier concentration [27]. The number of defects in the corrosion product films can infer the concentration of carriers, the electron conduction and mass transfer, these parameters are closely related to the further corrosion [28].

Table 7 shows the semiconductor parameters of the corrosion product films. With increase of tensile stress, the concentration of carriers also increases. Specifically, when plastic tensile strain (103%  $\sigma_s$ ) is loaded on P110 steels, the carriers’ concentration increases sharply. An order of magnitude difference is seen in the concentration of elastic loads. This phenomenon is related to the loaded tensile stress, which influences the grain size and defects of corrosion product films.

**Table 7.** Semiconductor parameters of corrosion products film on P110 steels in CO<sub>2</sub> environment induced by tensile stress

Tensile stress	Phase	Semiconductor or type	Flat band potential $E_{FB}/V$	Carriers concentration $N_A/cm^{-3}$
0% $\sigma_s$	FeCO <sub>3</sub>	P	-0.0326	$1.13 \times 10^{17}$
90% $\sigma_s$		P	-0.1593	$3.42 \times 10^{17}$
103% $\sigma_s$		P	-0.3781	$2.74 \times 10^{18}$

In 3.1, we discussed that the increase of tensile stress can make the grain size of corrosion product films becomes smaller, and the grain boundaries and micro-channels increase significantly. According to the point defect model (PDM) put forward by Macdonald [29], the induced tensile stress can be active electrochemical element to cause the rupture of passive films. Also the tensile stress can promote the disarray of local lattice on the defect structure of the passive films, and the presence of dislocations influences the acceptor densities of the oxide film [30]. Not only the Surface electrochemical activity of corrosion product films increased but also the defects structure of films

were expanded induced by tensile stress. This result in the anion resistance of corrosion product films decreases as well as flat band potential, and the ions that participated in the reaction are easier to enter the defects of the films, thus increasing carrier concentration. The results are in agreement with other reports [11,13,31]. Consequently, induced tensile stress has a negative effect on the protection of corrosion product films, and the likelihood of further corrosion increased, which is consistent with the regularities of EIS and polarisation curves.

#### 4. CONCLUSIONS

1 Induced tensile stress changes the time constant from one to two of the EIS measurement. Without tensile stress, only the capacitive reactance arc is seen in the Nyquist diagram. With induced tensile stress, a high-frequency capacitive reactance arc and a low-frequency capacitive reactance arc appeared. Meanwhile, the increase of stress will decrease the radii of the capacitive reactance arcs as well as the charge transfer resistance. Thus, the electrochemical reaction rate increased.

2 With the increase of induced tensile stress, the self-corrosion potential of P110 steels is negatively shifted, and the self-corrosion current density and the corrosion rate increased.

3 Induced tensile stress does not change the crystal type and semiconductor type of the corrosion product films formed on P110 steels in the CO<sub>2</sub> environment. The crystal types are all FeCO<sub>3</sub>, and the semiconductor types are all p-type.

4 Induced tensile stress can decrease the grain size of corrosion product films, which leads to more grain boundaries and micro-channels in the corrosion product films. Thus, the transfer ways of corrosive anions as well as the carrier concentration increased, thereby increasing the likelihood of further corrosion.

#### ACKNOWLEDGEMENTS

This work was financially supported by the National Natural Science Foundation of China (No. 51374180), and Key Laboratory Funding of Oil and Gas Materials of Sichuan Colleges (No. X151517KCL10).

#### References

1. S.D. Zhu, J.F. Wei, Z.Q. Bai, G.S. Zhou, J. Miao and R. Cai, *Eng. Fail. Anal.*, 18 (2011) 950.
2. L.M. Tavares, E.M.D. Costa, J.J.D.O. Andrade, R. Hubler and B. Huet, *Appl. Surf. Sci.*, 359 (2015) 143.
3. J.L. Li, H.X. Ma, S.D. Zhu, C.T. Qu and Z.F. Yin, *Corros. Sci.*, 86 (2014) 101.
4. S.D. Zhu, A.Q. Fu, J. Miao, Z.F. Yin, G.S. Zhou and J.F. Wei, *Corros. Sci.*, 53 (2011) 3156.
5. G.A. Zhang, D. Liu, Y.Z. Li and X.P. Guo, *Corros. Sci.*, 120 (2017) 107.
6. S. Nešić, *Corros. Sci.*, 49 (2007) 4308.
7. Z.X. Ren, X.D. Wu, G.Q. Han, L.Y. Liu, X.J. Wu, G.H. Zhang, H. Lin, J.M. Zhang and X.W. Zhang, *J. Petrol. Sci. Eng.*, 157 (2017) 1197.

8. Y.X. Wang, W.M. Zhao, H. Ai, X.G. Zhou and T.M. Zhang, *Corros. Sci.*, 53 (2011) 2761.
9. J.L. Tang, Z.H. Zhang, Y.Y. Wang, P.F. Ju, Y.M. Tang and Y. Zuo, *Corros. Sci.*, 135 (2018) 222.
10. J.B. Sun, G.A. Zhang, W. Liu and M.X. Lu, *Corros. Sci.*, 57 (2012) 131.
11. K. Gao, D. Li, X. Pang and S. Yang, *Corros. Sci.*, 52 (2010) 3428.
12. S.J. Kim, H.G. Jung and K.Y. Kim. *Electrochim. Acta.*, 78 (2012) 139.
13. S. Zhang, X.L. Pang, Y.B. Wang and K.W. Gao, *Corros. Sci.*, 75 (2013) 293.
14. ASTM G39-99. Standard Practice for Preparation and Use of Bent-Beam Stress-Corrosion Test Specimens. ASTM, (2011) West Conshohocken, America.
15. X. Li, F. Xie, D. Wang, C.H. Xu, M. W, D.X. Sun and J.J. Q, *Eng. Fail. Anal.*, 91 (2018) 275.
16. M.Y. Bao, C.Q. Ren, M.Y. Lei, X. Wang, A. Singh and X.Y. Guo, *Corros. Sci.*, 112 (2016) 585.
17. X.G. Feng, Y. Zuo, Y.M. Tang, X.H. Zhao and X.Y. Lu, *Electrochim. Acta.*, 58 (2011) 258.
18. R.H. Hausler and D.W. Stegmann, CO<sub>2</sub> Corrosion and Its Prevention by Chemical Inhibition in Oil and Gas Production, NACE International, St. Louis, America, 1988, 363.
19. D.H. Davies and G.T. Burstein, *Corrosion.*, 36 (1980) 416.
20. C.F. Chen, M.X. Lu, G.X. Zhao, Z.Q. Bai, M.L. Yan and Y.Q. Yang, *Acta Metall. Sin.*, 38 (2002) 411.
21. E.M. Gutmann, *Mechanochemistry of Solid Surface*, World Scientific Publishers, (1994) Singapore City, Republic of Singapore.
22. S. Sarkar and W. Aquino, *Electrochim. Acta.*, 111 (2013) 814.
23. A. Fattah-Alhosseini, *Arab. J. Chem.*, 9 (2016) S1342.
24. S.R. Morrison, *Electrochemistry at Semiconductor and Oxidized Metal Electrodes*, Plenum Press, (1988) City of New York, America.
25. C.Q. Ren, W.G. Wang, X. Jin, L. Liu and T.H. Shi, *RSC. Adv.*, 26 (2015) 20302.
26. Z.C. Feng, X.Q. Cheng, C.F. Dong, L. Xu and X.G. Li, *Corros. Sci.*, 52 (2010) 3646.
27. M.G. Mahjani, A. Ehsani and M. Jafarian, *Synth. Met.*, 160 (2010) 1252.
28. A. Fattah-Alhosseini, F. Soltani, F. Shirsalimi, B. Ezadi and N. Attarzadeh, *Corros. Sci.*, 53 (2011) 3186.
29. D.D. Macdonald, *Electrochim. Acta.*, 56 (2011) 1761.
30. C.M. Rangel, T.M. Silva and M.D.C. Belo, *Electrochim. Acta.*, 50 (2005) 5076.
31. P. Szroeder, I.Y. Sagalianov, T.M. Radchenko, V.A. Tatarenko, Y.I. Prylutsky and W. Strupiński, *Appl. Surf. Sci.*, 442 (2018) 185.